Modeling and Mitigating Noise and Nuisance Parameters in Received Signal Strength Positioning

Richard K. Martin, Amanda Sue King, Jason R. Pennington, Ryan W. Thomas, Russell Lenahan, and Cody Lawyer

***Abstract*—Localization via received signal strength (RSS) is often employed in cases where the received signal is fairly weak, either due to distance or due to deliberate covert operation or interference avoidance. However, most research on source localization via RSS implicitly assumes that the background noise is negligible, and that parameters of the transmitter and environment are known. Many commercial chipsets provide per-frame RSS measurements obtained when demodulating the signal, which do not include background noise; however, noise can still cause signal outages. In law enforcement, surveillance, and emergency situations, RSS may be obtained more crudely, such as by energy detection, in which case the RSS will include contributions from the background noise as well. This paper proposes new probabilistic RSS models that account for background noise in both types of RSS measurements. We also derive and evaluate maximum likelihood estimators (MLEs) for these new models, as well as for differential RSS, which has hitherto not been rigorously analyzed in the literature. Several of these MLEs are extended to estimate the transmit power and/or path loss if they are unknown. The new models are justified by extensive measured data.**

***Index Terms*—Noise floor, nuisance parameters, received signal strength, source localization.**

I. Introduction

Source localization, or geolocation, is the process of using a Wireless Sensor Network (WSN) to locate and track the position of a radio emitter [1]–[3]. Geolocation may be accomplished through Received Signal Strength (RSS), Angle of Arrival (AOA), Time of Arrival (TOA), and/or Time Difference of Arrival (TDOA) measurements [4], [5]. Though each measurement type has its own merits, this paper focuses on RSS, since we are interested in a large-scale deployment using many cheap sensors operating at low power. For comparison, AOA requires more complex hardware on each sensor (such as an antenna array), TOA requires cooperation between the emitter and sensors for precise timing, and TDOA requires bandwidth- and power-intensive cross-correlation between sensors.

Manuscript received December 09, 2011; revised April 05, 2012 and June 12, 2012; accepted June 12, 2012. Date of publication July 05, 2012; date of current version September 11, 2012. The associate editor coordinating the review of this manuscript and approving it for publication was Dr. Hing Cheung So. This work was supported in part by the Office of Naval Research. A portion of this paper appeared in the Proceeding of the International Conference on Acoustics, Speech, and Signal Processing, Prague, Czech Republic, May 2011. The views expressed in this paper are those of the authors, and do not reflect the official policy or position of the United States Air Force, Navy, Department of Defense, or the U.S. Government. This document has been approved for public release; distribution unlimited.

R. K. Martin, A. S. King, J. R. Pennington, R. W. Thomas, and C. Lawyer are with the Department of Electrical and Computer Engineering, The Air Force Inst. of Technology (AFIT), Wright-Patterson AFB, OH 45433 USA (e-mail: richard.martin@afit.edu; kingersue@gmail.com; jason.pennington@afit.edu; thomasrw@gmail.com; codylawyer@gmail.com).

R. Lenahan, deceased, was with the Department of Electrical and Computer Engineering, The Air Force Inst. of Technology (AFIT), Wright-Patterson AFB, OH 45433 USA.

Color versions of one or more of the figures in this paper are available online at http://ieeexplore.ieee.org.

Digital Object Identifier 10.1109/TSP.2012.2207118

In this paper, we are particularly interested in scenarios where the background noise must be taken into consideration and scenarios where the parameters of the emitter and environment are unknown to the sensors. Noise may be significant in cases where the emitter is weak and/or far from the sensors, and the nuisance parameters may be unknown when the emitter is owned and operated by a different entity than the WSN. Both scenarios often arise in applications in law enforcement, military reconnaissance, and emergency response.

There are two types of methods by which RSS measurements can be obtained: cooperative and non-cooperative [6]. In cooperative systems, such as cell phone handset geolocation by base stations, the device to be located may share information and parameter values with the WSN. In such cases, the reported RSS is just the signal power, as the digital signal can be demodulated and segregated from additive noise. In non-cooperative systems, such as locating emitters in a hostile environment, many properties of the emitter are unknown. In this case, the RSS may be determined by energy detection, such as by integrating the observed Power Spectral Density (PSD). In that case, the PSD will contain contributions from both the signal and background noise, and the RSS will be dominated by noise at low Signal to Noise Ratio (SNR) values. This paper treats these two approaches distinctly, since the effects of low signal power and of noise will be different between the two methods. We are primarily interested in the non-cooperative case, which is well suited to weak signals and unknown parameter values; however, the cooperative case is also formalized for comparison.

Most papers on RSS-based positioning largely ignore background noise and the ensuing range limitations. A notable exception is [7], which included a range limiting effect for cooperative RSS measurements, though with limited analysis. Non-reporting sensors were still included in the localization algorithm, since a non-report is still informative. However, the model and algorithm involved an implicit approximation which we will address here.

In non-cooperative scenarios, the transmitted power and the path loss exponent are typically not known *a priori*. In the literature, it is popular to omit the transmitted power from the model by using Differential Received Signal Strength (DRSS), wherein the original S RSS measurements are differenced to create $S-1$ DRSS measurements. Though this does reduce the parameter set, it complicates the probabilistic model, hence most papers on DRSS ignore probability and focus on geometric solutions with no guarantee of optimality. In fact, one of our goals is to show that the use of DRSS is not really a simplification when optimal algorithms are compared for both RSS and DRSS. In [8], a position estimate was obtained by "a weighted centroid method," and in [9] positioning was done via a Least Squares (LS) fit to the intersection of the circles produced by each distance measurement; neither approach is equivalent to a Maximum Likelihood Estimator (MLE). In [10], a gradient-descent approach yielded a non-linear LS solution, but the MLE and Cramer-Rao Lower Bound (CRLB) were not discussed. In [11], the closed-form LS solution was based on linearizing the problem; again, the MLE and CRLB were not discussed.

The contributions of this paper are as follows. (i) In Section II, we propose new probabilistic models to account for background noise in cooperative and non-cooperative RSS measurements, and we formalize the probabilistic model for DRSS (particularly the induced correlation between DRSS measurements). Experimental data is used to justify the models. (ii) Given these models, it is natural to derive the MLEs to estimate the transmitter position and nuisance parameters (transmitted power and path loss) under each of the models; this is done in Section III, which also includes a computational complexity comparison. We also show that our MLE for DRSS is mathematically equivalent to the LS DRSS algorithm of [10], [11], though our MLE formulation is computationally cheaper by about an order of magnitude. (iii) Given these new models and MLEs, is it natural to ask how the noise affects the Fisher information and CRLB regarding the position estimation; this is discussed in Section IV. In particular, we show that even when the transmit power and path loss are unknown, the MLEs for RSS and DRSS have comparable complexity and identical CRLBs, hence DRSS has no inherent advantage over RSS. (iv) In Section V, we use extensive simulations supported by some experimental data to quantify the performance of the proposed MLEs. Thus, the four contributions form a chain of: new models → new MLEs → theoretical performance analysis → numerical performance analysis.

Throughout, $(\,\cdot\,)^T$, $\mathrm{E}\{\,\cdot\,\}$, and $\langle\,\cdot\,\rangle$ denote matrix transpose, statistical expectation, and sample average, respectively. A vector Gaussian distribution is denoted $\mathbf{x} \sim \mathcal{N}(\mathrm{mean}, \mathrm{cov})$. Upper and lower case boldface quantities, e.g., $\mathbf{J}$ and $\mathbf{p}$, indicate matrices and column vectors, respectively. The matrices $\mathbf{0}$, $\mathbf{1}$, $\mathbf{I}$, contain all zeros, all ones, and the identity matrix, respectively; and when it is not clear from the context, they will be subscripted with their dimensionality. A hat (e.g., $\hat{x}$) indicates an estimate of its argument. Since base-10 and natural logs will occur frequently, we define $e_{\mathrm{dB}} = 10\log_{10}(e) \approx 4.343$.

II. System Model

In this section, we discuss the existing, standard RSS model and describe the layout of the WSN. We then extend the standard model to include the effects of background noise, with separate treatment for the cooperative and non-cooperative cases. Finally, we explicitly state the measurement model for DRSS.

A. Standard RSS Model

The transmitted power is σ_x^2, or $p_0 = 10\log_{10}\sigma_x^2$ in dB, as measured at a reference distance of $d_0 = 1$ m. The transmitted waveform is $x(t)$, the noise is $n(t)$ with power σ_n^2, and the received waveform is

$$y(t) = g_{\mathrm{tx}} g_{\mathrm{rx}} g_{\mathrm{pl}}\, x(t) \star h(t) + n(t). \tag{1}$$

Here, g_{tx} and g_{rx} are the scalar transmitter and receiver antenna voltage gains (which are random due to non-isotropic antenna radiation patterns), g_{pl} is the deterministic path loss factor, $h(t)$ models random constructive and destructive self-interference and shadowing in the multipath channel, $n(t)$ is Additive White Gaussian Noise (AWGN), and $\star$ denotes convolution. In general, all of the quantities in (1) except $x(t)$ depend on the sensor index s, but when it does not affect clarity, this index is omitted. The remainder of this section discusses the distribution of each of the gain factors and how they influence the RSS. We go into more detail than usual because it is necessary to have a solid model in order to account for the newly incorporated effects of background noise.

First, consider the deterministic path loss term, which models attenuation over distance. The WSN consists of S receiver nodes at known positions (x_s, y_s), for $s = 1, 2, \ldots, S$. The transmitter is at an unknown position (x_0, y_0), hence the transmitter-to-receiver distance is

$$d_s = \sqrt{(x_s - x_0)^2 + (y_s - y_0)^2}. \tag{2}$$

In linear scale, the path loss effects are given by

$$g_{\mathrm{pl}}^2 = \frac{\text{power at } d_s}{\text{power at } d_0} = \left(\frac{d_s}{d_0}\right)^{-\eta}, \tag{3}$$

where η is the path loss exponent. In free space, $\eta = 2$, but it may vary due to multipath and shadowing. It may be as large as 5 in dense urban environments [1], though the authors have typically seen values in $2 \lesssim \eta \lesssim 3$, and have observed even smaller values in indoor environments. In dB scale, the path loss term becomes

$$10\log_{10} g_{\mathrm{pl}}^2 = -\eta \overline{d}_s, \tag{4}$$

$$\overline{d}_s \triangleq 10\log_{10}(d_s/d_0), \tag{5}$$

as shown in the trend line in Fig. 1. The path loss slope and intercept, η and p_0, may be determined by calibration or included as nuisance parameters in the position estimation problem. In Fig. 1, the transmitter and receiver were Sun SPOTs. The SPOTs were kept in the same orientation for all measurements, so variations in the transmitter and receiver gains were minimal.

The RSS is the average power of the received signal. If $x(t)$ has a flat PSD, then

$$\sigma_y^2 = \frac{1}{T}\int |y(t)|^2\,dt \tag{6}$$

$$= g_{\mathrm{tx}}^2 g_{\mathrm{rx}}^2 g_{\mathrm{pl}}^2 \frac{1}{T}\int |x(t)|^2\,dt \int |h(\tau)|^2\,d\tau + \frac{1}{T}\int |n(t)|^2\,dt \tag{7}$$

$$= \sigma_x^2\, \underbrace{g_{\mathrm{pl}}^2 \cdot \left(g_{\mathrm{tx}}^2 g_{\mathrm{rx}}^2 g_{\mathrm{h}}^2\right)}_{g^2} + \sigma_n^2. \tag{8}$$

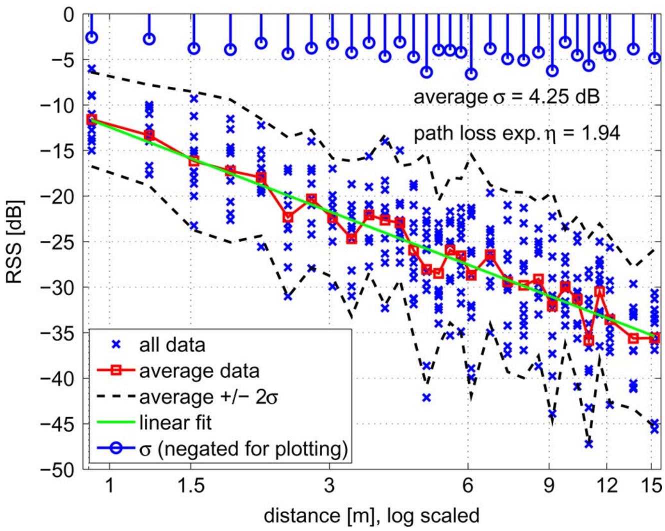

Fig. 1. Modeling the path loss g_{pl}^2. The upside-down stem plot at the top indicates the standard deviation of all of the RSS measurements at each distance. The transmitter and receiver orientations were fixed, hence the variation here is primarily due to shadowing and multipath.

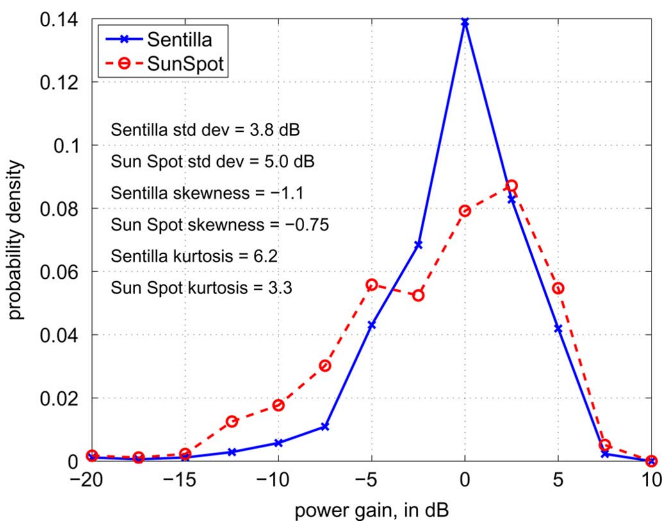

Fig. 2. Histograms of power gain g_{tx}^2 (or g_{rx}^2) measured at 700 different orientations, for Sentilla motes and Sun SPOTs.

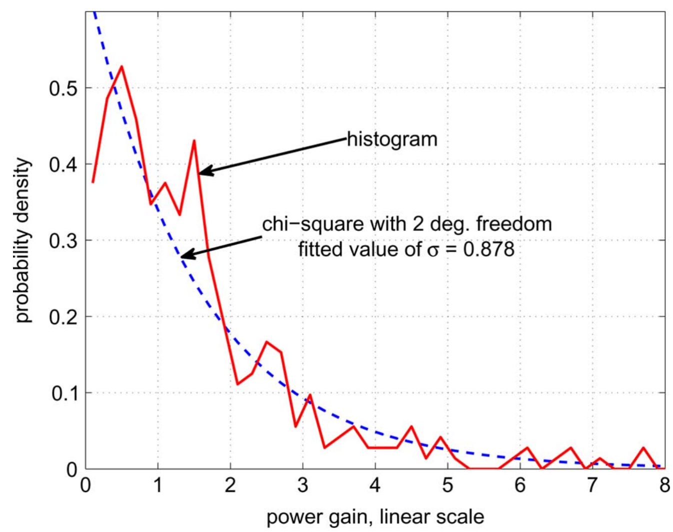

Fig. 3. Distribution of the channel power gain g_{h}^2, in linear scale. The data was obtained by computing statistics of the error in Fig. 1 relative to the linear fit. Using $\sigma = 0.878$ in the chi-square distribution leads to a good fit.

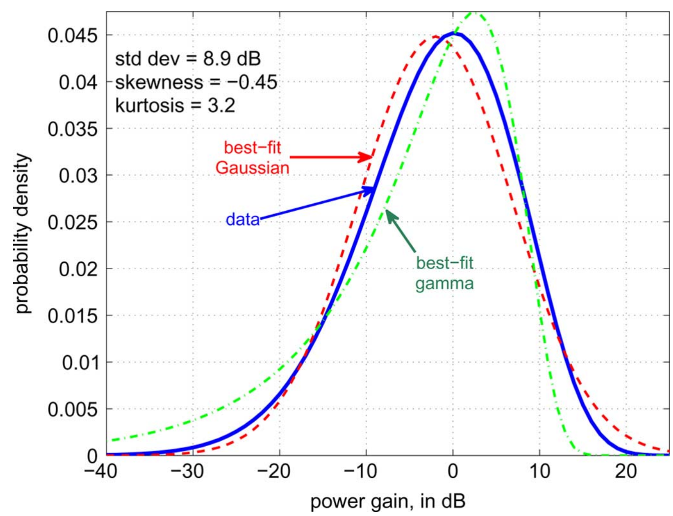

Fig. 4. Total power gain in dB, from convolving two of the Sun SPOT gain histograms from Fig. 2 with a Chi-square distribution with $\sigma = 1$, converted into dB.

where T is the total observation time per RSS measurement. For the remainder of this subsection, we simplify the discussion by using the assumptions in the standard RSS model; that is, we include the random fading from g^2 but not the noise from σ_n^2. However, we will reconsider additive noise in Sections II.B and II.C.

The overall power gain g^2 consists of three stochastic factors, g_{tx}^2, g_{rx}^2, and g_{h}^2; as well as the deterministic factor g_{pl}^2. In dB scale, the overall gain is a sum of these terms, hence its distribution is a convolution of the three individual distributions (shifted by the deterministic path loss term).

Regarding g_{tx}^2 and g_{rx}^2, even if antennas are designed to be roughly isotropic, many will have some variation in gain, making the gains dependent on the exact transmission angle. For example, commercially available Sentilla Motes and Sun SPOTs have power gains g^2 with standard deviations of 3.8 dB and 5.0 dB, respectively, as determined by measuring the gains at about 700 different orientations. Fig. 2 shows histograms of these values.

In environments with significant multipath, it is common for g_{h} to be modeled as a Rayleigh distribution, giving g_{h}^2 a chi-square distribution with two degrees of freedom ([12], p. 45). Fig. 3 shows a fit to this model, obtained by computing statistics of the error in Fig. 1 relative to the linear fit. Since the sensor orientations were held constant, the effects of g_{tx}^2 and g_{rx}^2 should be minimal, so that most of the variation is due to g_{h}. A chi-square distribution with a value of σ just below unity leads to a good fit.

Ignoring the deterministic path loss term for now, convolving dB scaled versions of g_{tx}^2, g_{rx}^2, and g_{h}^2 yields the total power gain. An example distribution determined in this fashion is shown in Fig. 4, where the transmitter and receiver were Sun SPOT sensor motes, and their measured gain patterns are as in Fig. 2; and the physical channel power gain was chi-square with $k = 2$ and $\sigma = 1$ (converted into dB scale before the convolution was performed). It is common in the literature to treat the overall gain as as log-normal (i.e., Gaussian in the dB domain) [1], [3], [13],

[14], [15]; though [16] examined the gamma distribution and the combination of a gamma and lognormal as alternatives. The model from our data in Fig. 4 shows some asymmetry (skewness), and the authors have often seen left-skewness in other RSS data collections. A Gaussian has no skewness and a pure gamma distribution shows too much skewness, hence a combination that is in-between the two is reasonable. However, the combination gamma-lognormal distribution has potentially 4 unknown parameters (shape and scale for the gamma and mean and variance for the lognormal), so hereafter we treat the RSS variations from fading as log-normal as it is a close fit and is much more analytically tractable.

Putting all of the gain terms together, the path loss term is deterministic and affects the mean RSS, whereas the remaining gain terms are stochastic and can be grouped together to form an approximately Gaussian distribution with an overall standard deviation of $\sigma_{\rm dB}$, leading to the standard RSS model

$$p_s = 10\log_{10}\sigma_y^2 \tag{9}$$
$$= \underbrace{10\log_{10}\sigma_x^2}_{p_0} + \underbrace{10\log_{10} g_{\rm pl}^2}_{-\eta\bar{d}_s} + \underbrace{10\log_{10}\left(g_{\rm tx}^2 g_{\rm rx}^2 g_{\rm h}^2\right)}_{w_s} \tag{10}$$
$$w_s \sim \mathcal{N}\left(0, \sigma_{\rm dB}^2\right). \tag{11}$$

This is consistent with the discussion above regarding Fig. 4. The shadowing levels are typically uncorrelated (with some exceptions [10], [17]), and the RSS is vectorized as

$$\mathbf{p} = [p_1, \ldots, p_S]^T \sim \mathcal{N}\left(\mathbf{m}, \sigma_{\rm dB}^2\mathbf{I}\right), \tag{12}$$
$$\mathbf{m} = [m_1, \ldots, m_S]^T, \tag{13}$$
$$m_s = p_0 - \eta\bar{d}_s. \tag{14}$$

Typically, $\sigma_{\rm dB}$ ranges from 4 dB to 12 dB, corresponding to uncluttered environments to environments with heavy shadowing [15]. However, as shown in Fig. 4, modest quality sensors can lead to a $\sigma_{\rm dB}$ of about 9 dB even in a benign channel.

B. Proposed Cooperative RSS Model

After (8), background noise was temporarily ignored. However, in reality, it leads to range limitations, whether the RSS measurements are obtained cooperatively or non-cooperatively. This was implicitly included in the model of [7], which was implicitly a cooperative model. We formalize the cooperative model here, based on [7], and the next section proposes the new non-cooperative model.

Most RSS-based location papers in the literature implicitly use cooperative measurements, wherein packets are fully demodulated, signal is separated from noise, and the chipsets provide per-frame RSS measurements based on the signal power only. The hardware that is usually referenced is IEEE 802.11a wireless LANs [2], [4], [18] or IEEE 802.15.4 sensor networks [5], [19]. The noise floor comes into play based on the fact that below some system-dependent SNR, the packets can no longer be demodulated, and the RSS becomes unavailable. Thus, in dB, the cooperative RSS is modeled as

$$p_{{\rm coop},s} = \begin{cases} p_s, & p_s \geq \tau_{\rm coop} \\ \text{NaN}, & p_s < \tau_{\rm coop} \end{cases} \tag{15}$$

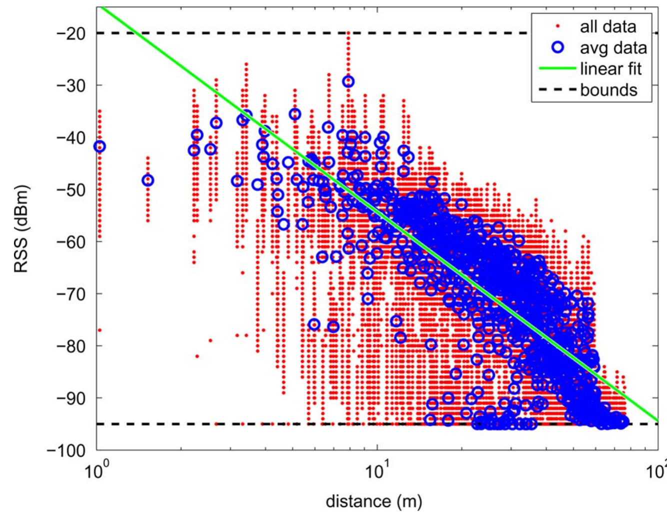

Fig. 5. Cooperative RSS data from IEEE 802.11a packets [20].

where $\tau_{\rm coop}$ is the lowest power level at which the packet can be demodulated, and NaN means "not a number," i.e., no RSS value was obtained. The dB power threshold $\tau_{\rm coop}$ roughly corresponds to a maximum range of [7]

$$d_{\max} \approx d_0 10^{(p_0 - \tau_{\rm coop})/(10\eta)}, \tag{16}$$

though longer ranges are possible due to the positive tail of the log-normal fading. Except in [7], this truncation effect appears to be ignored in the literature.

The model in (15) is supported by Fig. 5, which shows cooperatively measured RSS data obtained from IEEE 802.11 packets, downloaded from [20]. Each circle is the average of the 2000 measurements at that distance. The dashed lines at -20 dBm and -95 dBm indicate the largest and smallest RSS values seen in all 1.7 million data points. As the distance increases, packets falling below -95 dBm are lost, so in this case, $\tau_{\rm coop} = -95$ dBm.

C. Proposed Non-Cooperative RSS Model

In a non-cooperative system, there will be a noise floor, due to the fact that even if the gain g^2 drops with distance, the power in (8) will never drop below σ_n^2. The noise is often ignored in the literature, though [21] explicitly included it for acoustic RSS measurements. In the linear domain, $\sigma_x^2 g^2$ has a log-normal distribution and σ_n^2 has a chi-square distribution. These two quantities are independent, so the distribution of their sum (the RSS in linear scale) is the convolution of their two distributions. However, performing this convolution and converting to dB scale is analytically intractable.

A reasonable approximation of the non-cooperative RSS, including background noise and shadowing, is to add the means of the signal and noise in the linear domain,

$$\mathbf{p}_{\rm nc} \sim \mathcal{N}\left(\mathbf{m}_{\rm nc}, \sigma_{\rm dB}^2\mathbf{I}\right) \tag{17}$$
$$m_{{\rm nc},s} = 10\log_{10}(10^{m_s/10} + 10^{\tau_{\rm nc}/10}), \tag{18}$$

where $\tau_{\rm nc}$ is the average noise power in dB. A similar model accounting for background noise was given in [22], as

$$m_{{\rm nc},s}^{\rm asymptotes} = \begin{cases} m_s, & m_s \geq \tau_{\rm nc} \\ \tau_{\rm nc}, & m_s < \tau_{\rm nc} \end{cases}, \tag{19}$$

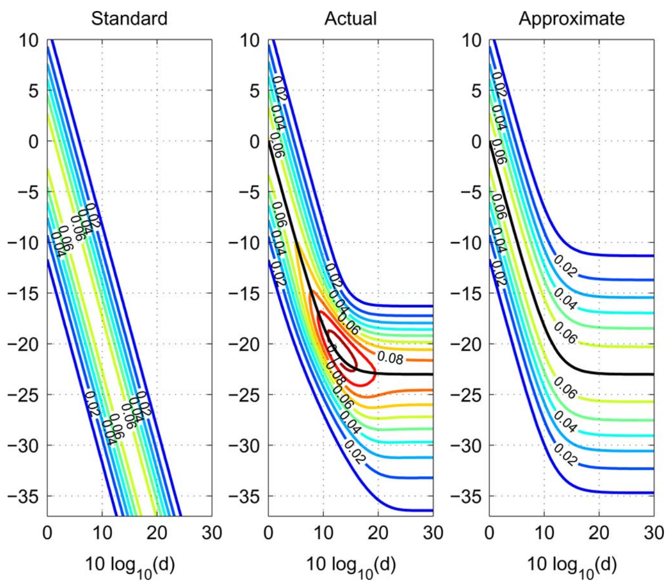

Fig. 6. Contours of the PDF of the standard model (12), the true model, and the proposed approximate model (17), assuming non-cooperative RSS measurement and noise at $\tau_{\rm nc} = -23$ dBm. The vertical axis is RSS in dBm.

with the same fading as (17). Note that (19) consists of the asymptotes of (18). However, we will use (18) in this paper as it is a better match to our experimental observations. Fig. 6 shows contours of the standard model without range limits from (12), the actual model (convolution of log-normal and chi-square, then converted to dB), and the approximation from (17)–(18). In each subplot, a vertical cross-section of the contours represents a Probability Density Function (PDF) of the RSS at that distance.

Note that the non-cooperative power threshold $\tau_{\rm nc}$ is different than the cooperative power threshold $\tau_{\rm coop}$. That is because $\tau_{\rm nc}$ is the power of the background noise, whereas $\tau_{\rm coop}$ is the lowest signal RSS that can be detected in the presence of noise.

The model in (17)–(18) is supported by Fig. 7, which shows non-cooperative data measured by the authors, with a short-range scenario in (a) and a long-range scenario in (b). The transmitter was a WARP FPGA board [23] and the receiver was a WiSpy [24]. The $\tau_{\rm nc}$ values are so different because the two tests were conducted about a year apart, using different transmitter and receiver gain settings. The trend lines shown in Fig. 7 were obtained by fitting p_0, η, and $\tau_{\rm nc}$ in (18).

D. Differential RSS Model

The DRSS is obtained by subtracting pairs of RSS measurements. While there are $S(S-1)$ possible ordered pairs of RSS values, the resulting DRSS values could all be obtained from linear combinations of $S-1$ of them. Thus, for simplicity, we only consider the DRSS measurements

$$q_s = p_s - p_S, \quad s \in \{1, \ldots, S-1\}. \tag{20}$$

Observe that if background noise is ignored, p_0 cancels out,

$$\begin{aligned} \mathrm{E}\left\{q_s\right\}\big|_{\tau_{\rm nc}\to-\infty} &= (p_0 - \eta \overline{d}_s) - (p_0 - \eta \overline{d}_S) \quad &(21)\\ &= \eta \cdot (\overline{d}_S - \overline{d}_s), &(22)\end{aligned}$$

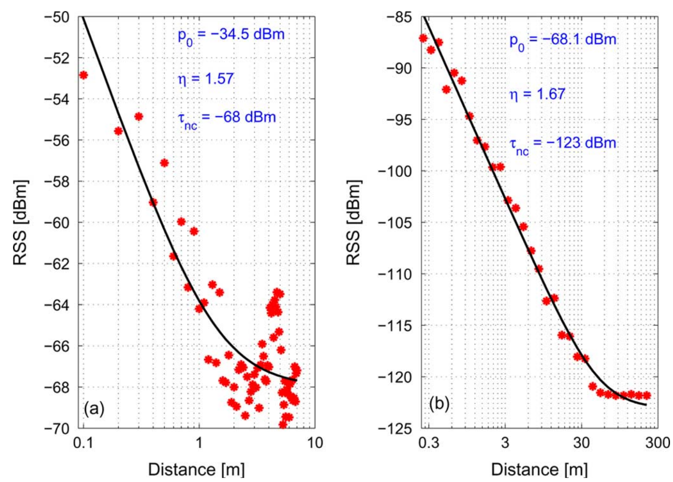

Fig. 7. Non-cooperative RSS data using a WARP FPGA board [23] as transmitter and a WiSpy [24] as receiver. (a) was a short-range scenario and (b) was a long-range scenario, since the transmitter and receiver had different gains and settings between the two tests.

but this does not happen if the background noise is included via (18) or (19).

Three issues motivate a more rigorous comparison of RSS and DRSS. First, the vector of DRSS values $\mathbf{q}$ is $(S-1)\times 1$, whereas the vector of RSS values $\mathbf{p}$ is $S \times 1$. Second, even if the RSS values are uncorrelated, the DRSS values become correlated, since they all depend on p_S:

$$\begin{aligned} \mathbf{C}_p &= \mathrm{E}\{\mathbf{p}\mathbf{p}^T\} = \sigma_{\rm dB}^2 \mathbf{I}_S, &(23)\\ \mathbf{C}_q &= \mathrm{E}\{\mathbf{q}\mathbf{q}^T\} = \sigma_{\rm dB}^2 \left(\mathbf{I}_{S-1} + \mathbf{1}_{S-1,1}\mathbf{1}_{S-1,1}^T\right), &(24)\\ \mathbf{C}_q^{-1} &= \sigma_{\rm dB}^{-2}\left(\mathbf{I}_{S-1} - S^{-1}\mathbf{1}_{S-1,1}\mathbf{1}_{S-1,1}^T\right). &(25)\end{aligned}$$

Third, once the background noise is included, p_0 no longer cancels out, so forcing it to cancel is an approximation. We will investigate these three issues in Section IV.B.

The inverse of $\mathbf{C}_q$ will be used later for the MLE and CRLB derivations, and it is obtainable via the Sherman-Morrison formula (which is a special case of the Woodbury formula, sometimes called the matrix inversion formula or the ABCD lemma) [25].

III. Algorithms

Section II proposed new stochastic models for cooperatively measured RSS and non-cooperatively measured RSS. We also reviewed the previously-proposed DRSS model. In this section, we derive the MLEs for these three models, defined as [26]

$$\begin{aligned} \hat{\mathbf{z}}_{\rm ML} &= \arg\max_{\mathbf{z}} \mathcal{L} &(26)\\ \mathcal{L} &= \ln f(\mathbf{r}\,|\,\mathbf{z}) &(27)\end{aligned}$$

where $\mathbf{z}$ contains the unknowns and $\mathbf{r}$ is the measurement vector ($\mathbf{p}$ for RSS or $\mathbf{q}$ for DRSS). In Section III.D, we show that the MLE for DRSS is mathematically equivalent to but computationally cheaper than the LS solution for DRSS of [10], [11].

A. Standard RSS and Non-Cooperative RSS

In the standard model of (12), the RSS has a normal distribution in dB. The only difference in the proposed non-cooperative model in (17) is the functional form of the mean. Thus, both cases share a similar form for the MLE, given generically by ([26], p.254)

$$\mathbf{p} \sim \mathcal{N}\left(\mathbf{m}(\mathbf{z}), \sigma_{\mathrm{dB}}^2 \mathbf{I}\right) \tag{28}$$
$$\hat{\mathbf{z}}_{\mathrm{ML}} = \arg\min_{\mathbf{z}} \|\mathbf{p} - \mathbf{m}(\mathbf{z})\| \tag{29}$$

The measured RSS vector is $\mathbf{p}$ and the mean vector $\mathbf{m}$ is from (13) for the standard case or from (18) for the non-cooperative case.

Equation (28) can be solved via Newton-Raphson or other search procedures, but for simplicity we assume a 2D grid search over (x_0, y_0). However, notice that in the standard model, p_0 and η appear linearly in $\mathbf{m}$. Thus, for each candidate position guess $(\tilde{x}_0, \tilde{y}_0)$, the estimates of p_0 and η can be computed in closed form ([26], p.223), [27], though they will be dependent on $(\tilde{x}_0, \tilde{y}_0)$. By differentiating the log-likelihood of (28) with respect to p_0 and η, setting the results to zero and solving (details omitted to save space), we obtain

$$\begin{bmatrix} \widehat{p_0} \\ \widehat{\eta} \end{bmatrix} = \begin{bmatrix} 1 & -\langle \overline{d}_s(\tilde{x}_0, \tilde{y}_0) \rangle \\ \langle \overline{d}_s(\tilde{x}_0, \tilde{y}_0) \rangle & -\left\langle \overline{d}_s^2(\tilde{x}_0, \tilde{y}_0) \right\rangle \end{bmatrix}^{-1} \begin{bmatrix} \langle p_s \rangle \\ \langle p_s \overline{d}_s \rangle \end{bmatrix} \tag{30}$$

where $\langle \cdot \rangle$ denotes an average over s. The resulting distribution without nuisance parameters is sometimes called the concentrated likelihood or the profile likelihood, which reduces (29) to

$$(\hat{x}_0, \hat{y}_0) = \arg\min_{x_0, y_0} \left\| \mathbf{p} - [\mathbf{1}, \overline{\mathbf{d}}] \begin{bmatrix} \widehat{p_0} \\ \widehat{\eta} \end{bmatrix} \right\|, \tag{31}$$

where $\widehat{p_0}$ and $\widehat{\eta}$ are as in (30). Thus, the overall approach is to perform a 2D grid search over (x_0, y_0), use (30) to estimate (p_0, η) at each grid point, and pick the grid point satisfying (29), as in ([26], p.257), [27]. The resolution of the grid will potentially limit the quality of the solution, though we have not observed this to be a significant problem.

However, in the new non-cooperative RSS model, p_0 and η no longer appear linearly in $\mathbf{m}$. Thus, if they are unknown, solving for them requires a grid search for optimality ([26], p.177), or a Newton-Raphson (or similar) search procedure.

B. Cooperative RSS

Based on (15), the distribution of cooperative RSS is continuous above τ_{coop} and discrete for $p = \mathrm{NaN}$. This was dealt with incorrectly in [7], which combined contributions to the log-likelihood function from both a probability density and from probabilities. Casting the resulting MLE in our notation and setting $\mathbf{z} = [x_0, y_0]^T$ yields

$$\hat{\mathbf{z}}_{\mathrm{ML}} = \arg\min_{\mathbf{z}} L \tag{32}$$
$$L = \frac{1}{2\sigma_{\mathrm{dB}}^2} \sum_{s: p_s \neq \mathrm{NaN}} [p_s - m_s(\mathbf{z})]^2 - \sum_{s: p_s = \mathrm{NaN}} \ln Q\left(\frac{m_s(\mathbf{z}) - \tau_{\mathrm{coop}}}{\sigma}\right) \tag{33}$$

To avoid the use of a mixed distribution and the resulting improper MLE formulation, note that the RSS is typically quantized, such as to the nearest integer value. Thus, we can use a fully discrete distribution for cooperative RSS, as quantized to values in the set $\{\rho_k = \rho_{\min} + k\Delta\}$, [see (34) and (35) shown at the bottom of the page]. The $\hat{\mathbf{z}}$ that maximizes either L or $\mathcal{L}$ must be computed numerically; again, we favor a 2D grid search for simplicity of presentation.

Observe that integrating a PDF across unit-width bins will convert its values to probabilities, and that the heights of samples of the PDF are often good approximations to these probabilities. Thus, the approach in [7] could be viewed as an approximation to the true MLE. In fact, for most realistic parameter values, the Root Mean Squared Error (RMSE) values of the approximate MLE and the true MLE are almost identical (within 2% or less). Thus, in Section V we will not make a further distinction between our cooperative MLE and that of [7]. However, this section is primarily included in this paper for comparison, since we are more interested in the non-cooperative case.

C. MLE for DRSS

The DRSS measurements are correlated, so

$$\mathbf{q} \sim \mathcal{N}(\mathrm{E}\{\mathbf{q}\}, \mathbf{C}_q) \tag{36}$$
$$\hat{\mathbf{z}}_{\mathrm{ML}} = \arg\min_{\mathbf{z}} (\mathbf{q} - \mathrm{E}\{\mathbf{q}\})^T \mathbf{C}_q^{-1} (\mathbf{q} - \mathrm{E}\{\mathbf{q}\}) \tag{37}$$
$$= \arg\min_{\mathbf{z}} (S \cdot \|\mathbf{q} - \mathrm{E}\{\mathbf{q}\}\|^2 - [(\mathbf{q} - \mathrm{E}\{\mathbf{q}\})^T \mathbf{1}]^2) \tag{38}$$
$$\mathrm{E}\{q_s\} = m_{\mathrm{nc},s}(\mathbf{z}) - m_{\mathrm{nc},S}(\mathbf{z}), \tag{39}$$

with $\mathbf{C}_q^{-1}$ from (25). Again, (38) could be minimized by a variety of methods, and we use a 2D grid search over (x_0, y_0) for simplicity of presentation here.

The LS solutions in [10], [11] were similar to (37) but with $\mathbf{C}_q^{-1}$ omitted, and [10] summed over all $S(S-1)/2$ DRSS redundant values rather than just the $S-1$ linearly independent measurements. However, as will be shown in Section III.D,

$$\mathcal{L} = \ln \prod_{s=1}^{S} \mathrm{P}[p_s \mid \mathbf{z}] \tag{34}$$

$$\mathrm{P}[p_s = \rho_k \mid \mathbf{z}] = \begin{cases} Q\left(\frac{\rho_k - m_s(\mathbf{z}) - \Delta/2}{\sigma}\right) - Q\left(\frac{\rho_k - m_s(\mathbf{z}) + \Delta/2}{\sigma}\right), & \rho_k \geq \tau_{\mathrm{coop}} \\ 1 - Q\left(\frac{\tau_{\mathrm{coop}} - m_s(\mathbf{z}) - \Delta/2}{\sigma}\right), & \rho_k = \mathrm{NaN} \end{cases} \tag{35}$$

the LS and MLE approaches lead to mathematically equivalent solutions, though the LS implementation is considerably more computationally expensive.

The benefit of DRSS is that in the absence of background noise, p_0 cancels out of the model. However, in the presence of background noise, it does not. Thus, DRSS implicitly requires one to use the standard model that ignores noise. Assuming that this is done, we can ignore p_0 and estimate η similarly to (30). This involves differentiating the log-likelihood of (36) with respect to η, setting the results to zero, and solving, all as a function of the candidate position guess $(\tilde{x}_0, \tilde{y}_0)$. This results in

$$\widehat{\eta} = \frac{\langle q_s \rangle \langle \overline{d}_s - \overline{d}_S \rangle - \langle q_s (\overline{d}_s - \overline{d}_S) \rangle}{\langle (\overline{d}_s - \overline{d}_S)^2 \rangle - \langle \overline{d}_s - \overline{d}_S \rangle^2} \tag{40}$$

where the sample averages are over $1 \leq s \leq S-1$ and each $\overline{d}_s$ is a function of the tentative grid points of $(\tilde{x}_0, \tilde{y}_0)$.

D. Equivalence of DRSS Algorithms

In this section, we prove that the LS DRSS algorithm in [10], [11] is mathematically equivalent to our MLE algorithm for DRSS. We then list the computational complexity for all algorithms in this section, and in particular we note that the complexity of the direct MLE implementation for DRSS is much less than that of the LS implementation. To clarify, it is well-known that the MLE for a signal in the presence of additive Gaussian noise leads to a non-linear LS solution [26], but that equivalence is not what we are demonstrating. Rather, we are showing that the MLE using $S-1$ non-redundant DRSS measurements with all correlation terms accounted for is equivalent to the LS solution of [10], [11] which uses all $S(S-1)/2$ redundant RSS measurements but does not account for the correlation between measurements.

The LS DRSS solution from [10], [11] can be written as

$$\hat{\mathbf{z}}_{\mathrm{ML}} = \arg\max_{\mathbf{z}} \mathcal{L}_{\mathrm{LS}} \tag{41}$$

$$\mathcal{L}_{\mathrm{LS}} = \sum_{k<l} \Delta_{k,l}^2 \tag{42}$$

$$\Delta_{k,l} \triangleq (p_k - p_l) - \mathrm{E}\{p_k - p_l\} \tag{43}$$

$$= (p_k - p_l) - \eta(\overline{d}_l - \overline{d}_k). \tag{44}$$

Noting that $\Delta_{l,k}^2 = \Delta_{k,l}^2$ and that $\Delta_{k,k}^2 = 0$, we can extend the double summation over all k and l as

$$\mathcal{L}_{\mathrm{LS}} = \frac{1}{2} \sum_{k,l=1}^{S} \Delta_{k,l}^2 \tag{45}$$

Noting that $\Delta_{k,l} = \Delta_{k,S} - \Delta_{l,S}$,

$$\mathcal{L}_{\mathrm{LS}} = \frac{1}{2} \sum_{k,l=1}^{S} \left(\Delta_{k,S}^2 + \Delta_{l,S}^2 - 2\Delta_{k,S}\Delta_{l,S} \right) \tag{46}$$

$$= \frac{S}{2} \sum_{k=1}^{S} \Delta_{k,S}^2 + \frac{S}{2} \sum_{l=1}^{S} \Delta_{l,S}^2 - \sum_{k,l=1}^{S} \Delta_{k,S}\Delta_{l,S} \tag{47}$$

$$= S \sum_{k=1}^{S} \Delta_{k,S}^2 - \left(\sum_{k=1}^{S} \Delta_{k,S} \right)^2 \tag{48}$$

$$= \mathcal{L}_{\mathrm{MLE}}, \tag{49}$$

TABLE I

COMPUTATIONAL COMPLEXITY PER (x_0, y_0) GRID POINT. S IS THE TOTAL NUMBER OF SENSORS AND N IS THE NUMBER THAT REPORT "NAN" IN THE COOPERATIVE CASE. FOR p_0 AND η, K/U INDICATE WHETHER THEY CAN BE CONSIDERED KNOWN OR UNKNOWN. "LEQ" COUNTS LOG, EXPONENTIAL, OR Q-FUNCTION CALLS

algorithm	p_0	η	$\times$	$\pm$	$\div$	LEQ
standard RSS	k/u	k	$4S$	$6S$	0	S
	k/u	u	$6S$	$8S$	0	S
non-coop.	k	k	$5S$	$6S$	S	$2S$
cooperative	k	k	$4S$	$9S-N$	0	$4S-N$
apprx.coop.[7]	k	k	$4S$	$4S$	0	$2S+N$
LS DRSS [11]	u	k	$\frac{1}{2}S^2$	$\frac{3}{2}S^2$	0	S
MLE DRSS	u	k	$4S$	$6S$	0	S
	u	u	$6S$	$9S$	0	S

where the last line refers to the cost function within (38). Thus, for DRSS, the LS and MLE cost functions are the same.

The computational complexity of the algorithms in this section is listed in Table I. The table assumes the use of the most efficient implementation we could produce. Only the highest order terms are shown in Table I, but including second-order terms, the LS DRSS algorithm requires $\frac{1}{2}S^2 + \frac{7}{2}S$ multiplies, whereas the MLE DRSS implementation only uses $4S$ multiplies (all per grid point). For $S = 75$, for example, the direct MLE implementation is about 10 times cheaper.

IV. INFORMATION ANALYSIS

In this section, we first analyze the loss in Fisher information due to the noise floor, for both the new cooperative and non-cooperative models, with the goal of showing that the noise explicitly provides a range limitation, allowing for an infinite grid analysis that is not possible when using the standard model. The point of an infinite grid model is to assess performance independent of the exact number and geometry of sensors, which yields simple formulas showing the effect of the sensor spacing. Next, we show that the CRLBs for RSS and DRSS are identical in the absence of noise, but differ very slightly when noise is included. This reinforces our unorthodox belief that DRSS is inherently no better or worse than RSS (in terms of analytic simplicity, computational complexity, and performance), even when p_0 is unknown.

The tools we use in this section are the Fisher Information Matrix (FIM) and its inverse, the CRLB. The FIM is a measure of how much information an observation vector $\mathbf{r}$ (set to $\mathbf{p}$ or $\mathbf{q}$ later in this section) contains about a parameter vector $\mathbf{z}$ that is to be estimated. The CRLB is a lower bound on the covariance of any unbiased estimator of $\mathbf{z}$. The FIM, $\mathbf{J}$, and the CRLB, $\mathbf{J}^{-1}$, are given by

$$\mathcal{L} = \ln f(\mathbf{r} \,|\, \mathbf{z}), \tag{50}$$

$$J_{i,j} = -\mathrm{E}\left\{ \frac{\partial \mathcal{L}}{\partial z_i} \frac{\partial \mathcal{L}}{\partial z_j} \right\}, \tag{51}$$

$$\mathrm{COV}[\mathbf{z}] \geq \mathbf{J}^{-1}. \tag{52}$$

If $\mathbf{r} \sim \mathcal{N}(\mathrm{E}\{\mathbf{r}\}, \mathrm{COV}[\mathbf{r}])$, as is the case in this paper, then [26]

$$\mathbf{J} = \mathbf{G}^T (\mathrm{COV}[\mathbf{r}])^{-1} \mathbf{G}, \tag{53}$$

$$\mathbf{G}^T = \nabla_{\mathbf{z}} \mathrm{E}\{\mathbf{r}^T\}. \tag{54}$$

A. Information Degradation by Noise

The effects of the range limits of the previous section will cause a loss of information in the WSN. In this section, we quantify this. While the unknowns are x_0 and y_0, all of the information provided by p_s is available in the distance d_s. Thus, for simplicity, in this section we will first consider the information about the scalar d_s contained in the scalar p_s, though later we will consider the overall information on positioning accuracy.

By (53), the Fisher information about d_s contained in an RSS observation p_s is

$$J_s\left(p_s\,|d_s\right) = \frac{1}{\sigma^2}\left(\frac{\partial m_s}{\partial d_s}\right)^2. \tag{55}$$

Depending on whether we use the RSS model of (12), (15), or (17), the bound will change. For the standard model of (12) and the non-cooperative model of (17), all that changes is the mean. In the cooperative case of (15), we can use the Modified CRLB (MCRLB) [28] to approximate the CRLB, with a potentially looser bound. In the MCRLB, a modified Fisher information is obtained by conditioning on and later averaging over unknown nuisance parameters. In our case, we will treat random outages (occurrences of "NaN") as a nuisance parameter. From (15), the probability of an outage is

$$\mathrm{P}[\text{outage}] = Q((p_0 - \eta\overline{d}_s - \tau_{\text{coop}})/\sigma), \tag{56}$$

where the Q function $Q(\,\cdot\,)$ is the integral of a unit Gaussian above its argument. When there is no outage, the Fisher information is identical to that of the standard case; and when there is an outage, there is no Fisher information conveyed. (In Shannon's sense, there is information, insofar as we suspect the distance is large when there are outages; but the Fisher information only deals with the local curvature of the log-likelihood ([5], p.62).) Thus, the Fisher information for the three cases can be shown to be

$$J_s = \left(\frac{\eta e_{\text{dB}}}{\sigma d_s}\right)^2 \cdot \alpha_s, \tag{57}$$

$$\alpha_s = \begin{cases} 1, & \text{standard} \\ 1 - Q((p_0 - \eta\overline{d}_s - \tau_{\text{coop}})/\sigma), & \text{coop.} \\ \left(\frac{10^{m_s/10}}{10^{m_s/10}+10^{\tau_{\text{nc}}/10}}\right)^2, & \text{non-coop.} \end{cases} \tag{58}$$

with J_s in units of meters^{-2}. Alternatively, to avoid use of the MCRLB for the cooperative case, one could differentiate the quantized RSS from (35), similar to [13] which used "connectivity," which was a binary quantized RSS.

Even without background noise, the utility of RSS measurements drops with distance. However, when including the effects of noise, the drop off is much more drastic beyond the cut-off region. Specifically, the Fisher information of the standard model is further degraded by factor α_s that drops monotonically from one to zero as the distance ranges from zero to infinity. Fig. 8(a) shows the RSS and Fig. 8(b) shows the corresponding Fisher information (rather, its square root, in meters^{-1}). These plots used $\eta = 2$, $\sigma = 4$ dB, $p_0 = 0$ dBm, $\tau_{\text{coop}} = -30$ dBm, and $\tau_{\text{nc}} = -30$ dBm.

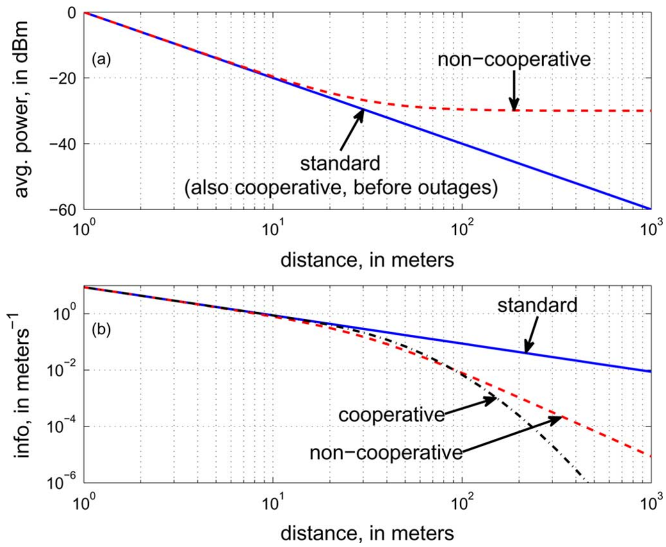

Fig. 8. The effects of modeling a noise floor in the RSS. In (a), the cooperative model is identical to the standard model above −30 dBm, but then it gradually disappears due to random outages.

Now we return to the full positioning problem. For purposes of gaining intuition, consider an infinite grid of sensors, in concentric rings about the true source location. The spacing between rings is Δ meters, with approximately the same spacing between sensors on each ring. (This is an approximation of a regularly spaced grid with one sensor per Δ^2 meters^2.) Referring to (54),

$$\mathbf{G}^T = \begin{bmatrix} \frac{\partial}{\partial x_0}\mathbf{m}^T \\ \frac{\partial}{\partial y_0}\mathbf{m}^T \end{bmatrix} = -\eta \begin{bmatrix} \frac{\partial}{\partial x_0}\overline{\mathbf{d}}^T \\ \frac{\partial}{\partial y_0}\overline{\mathbf{d}}^T \end{bmatrix}. \tag{59}$$

Applying (53) and noting that $\frac{\partial d_s}{\partial x_0} = -\sin\theta_s$ and $\frac{\partial d_s}{\partial y_0} = -\cos\theta_s$, we have

$$\mathbf{J}_{\text{standard}} = \left(\frac{\eta e_{\text{dB}}}{\sigma}\right)^2 \times \begin{bmatrix} \sum_s d_s^{-2}\cos^2\theta_s, & 0 \\ 0, & \sum_s d_s^{-2}\sin^2\theta_s \end{bmatrix} \tag{60}$$

We can replace the sum over s by a dual sum, first around each ring and then over the rings. Per ring, there are $N_{\text{ring}} \approx 2\pi d_{\text{ring}}/\Delta$ sensors, and the sum of the $\sin^2$ and $\cos^2$ terms become $N_{\text{ring}}/2$. Thus,

$$\mathbf{J}_{\text{standard}} \approx \left(\frac{\eta e_{\text{dB}}}{\sigma}\right)^2 \frac{\pi}{\Delta} \sum_{\text{ring } i} d_{\text{ring } i}^{-1}\mathbf{I}_2 = \left(\frac{\eta\sqrt{\pi}e_{\text{dB}}}{\sigma\Delta}\right)^2 \sum_{i=1}^{\infty} \frac{1}{i}\mathbf{I}_2 \tag{61}$$

The harmonic series $\sum_i i^{-1}$ diverges, hence *an infinite grid analysis is not possible in the standard case*. However, if we consider the effects of the noise floor in the non-cooperative case, the sums in (60) and (61) get additional factors of α_i as in (57):

$$\mathbf{J}_{\text{noncoop}} \approx \left(\frac{\eta\sqrt{\pi}e_{\text{dB}}}{\sigma\Delta}\right)^2 \sum_{i=1}^{\infty} \frac{1}{i}\alpha_i^{\text{nc}}\mathbf{I}_2. \tag{62}$$

As we are concerned with limiting effects, consider large distances. Observe that

$$\sqrt{\alpha_i^{\mathrm{nc}}} = \frac{10^{m_s/10}}{10^{m_s/10} + 10^{\tau_{\mathrm{nc}}/10}}, \tag{63}$$

$$\lim_{d_i\to\infty} \sqrt{\alpha_i^{\mathrm{nc}}} = \frac{10^{m_s/10}}{10^{\tau_{\mathrm{nc}}/10}} = \underbrace{10^{(p_0-\tau_{\mathrm{nc}})/10}}_{\text{margin}} \cdot d_i^{-\eta}, \tag{64}$$

though at finite distances, it is smaller than this. The first factor is the margin between p_0 and the noise floor, converted to linear scale. Applying this to (62),

$$\mathbf{J}_{\mathrm{noncoop}} \lesssim \left(\frac{\eta\sqrt{\pi}e_{\mathrm{dB}}\mathrm{margin}}{\sigma\Delta^{1+\eta}}\right)^2 \sum_{i=1}^{\infty} i^{-1-2\eta}\mathbf{I}_2. \tag{65}$$

Now the summation is the P-series, also called the Riemann Zeta function [29], which converges for all $\eta > 0$. For $\eta = 1$ (at the very low end of typical numbers), the summation is ≈ 1.202, and it drops monotonically to one as η increases. Thus, the square root of the CRLB (in order to get units of distance) is

$$\boxed{\sqrt{\mathrm{COV}}\left\{\begin{bmatrix} x_0 \\ y_0 \end{bmatrix}\right\} \geq \sqrt{\mathbf{J}_{\mathrm{noncoop}}^{-1}} \gtrsim \frac{\sigma\Delta^{1+\eta}}{\eta\sqrt{\pi}e_{\mathrm{dB}}\mathrm{margin}}\mathbf{I}_2.} \tag{66}$$

This formula is useful because it gives an idea of how the sensor spacing Δ affects positioning performance in a very large grid, with no geometric terms left in the result.

In the cooperative case, the sums in (60) and (61) again get additional factors of α_i as in (62):

$$\mathbf{J}_{\mathrm{coop}} \approx \left(\frac{\eta\sqrt{\pi}e_{\mathrm{dB}}}{\sigma\Delta}\right)^2 \sum_{i=1}^{\infty} \frac{1}{i}\alpha_i^{\mathrm{coop}}\mathbf{I}_2. \tag{67}$$

It is fairly easy to bound the summation in (67) to prove that it converges. However, the authors have not been able to find a bound that is tight enough to provide any meaningful intuition.

B. Information in RSS vs. DRSS

Recall that DRSS introduces measurement correlation and involves $S-1$ observations rather than S, which suggests possible performance differences between RSS and DRSS. Here, we show that when background noise is ignored the CRLB on (x_0, y_0) is identical for RSS and DRSS, and when including background noise, DRSS does induce a small loss of information, which vanishes as $S \to \infty$. This all holds whether η is known or not.

A similar comparison was developed in [14]. The distinction is that [14] assumes that only (x_0, y_0) are unknown and that p_0 is precalibrated for RSS but unknown for DRSS, whereas we consider (x_0, y_0, p_0) to all be unknown for both measurement types. Thus, under the assumptions of [14], $\mathrm{CRLB}_{\mathrm{RSS}} \leq \mathrm{CRLB}_{\mathrm{DRSS}}$ (with equality in very special geometries); whereas we show that when (x_0, y_0, p_0) are all unknown in both RSS and DRSS scenarios, the 2×2 (x_0, y_0) submatrices of the full CRLBs are equal for all geometries. Moreover, we extend the analysis to our new model and include η as an additional unknown in both cases.

Let the potential unknowns be

$$\mathbf{z} = [x_0, y_0, \eta, P_0]^T. \tag{68}$$

It will be useful to define the scalar

$$\gamma_s \triangleq \sqrt{\alpha_s} = \frac{\partial m_{\mathrm{nc},s}}{\partial m_s}, \tag{69}$$

which is given by (58). Notably, it is unity when background noise is ignored ($\tau \to -\infty$). The resulting FIM for RSS is a generalization of the well-known bound for the noiseless case,

$$\mathbf{J} = \sigma_{\mathrm{dB}}^{-2}\mathbf{G}^T\mathbf{G} \tag{70}$$

$$\mathbf{G}^T \triangleq \nabla_{\mathbf{z}}\mathrm{E}\{\mathbf{p}^T\} = [\mathbf{g}_1, \mathbf{g}_2, \ldots, \mathbf{g}_S] \tag{71}$$

$$\mathbf{g}_s \triangleq \gamma_s\left[\frac{e_{\mathrm{dB}}\eta}{d_s^2}(x_s - x_0), \frac{e_{\mathrm{dB}}\eta}{d_s^2}(y_s - y_0), -\overline{d}_s, 1\right]^T,$$

with γ_s being the only new addition thus far.

For DRSS, we will treat the observations as the $(S-1)\times 1$ vector $\mathbf{q}$ rather than the $S\times 1$ vector $\mathbf{p}$. In the absence of noise, we can (and in fact, must) omit p_0 from $\mathbf{z}$. The gradient matrix $\mathbf{G}_q$ is now slightly different,

$$\begin{aligned}\mathbf{G}_q^T &\triangleq \nabla_{\mathbf{z}}\mathrm{E}\{\mathbf{q}^T\} \\ &= [\mathbf{g}'_1 - \mathbf{g}'_S, \mathbf{g}'_2 - \mathbf{g}'_S, \ldots, \mathbf{g}'_{S-1} - \mathbf{g}'_S] \\ \mathbf{g}'_s &\triangleq \left[\frac{e_{\mathrm{dB}}\eta}{d_s^2}(x_s - x_0), \frac{e_{\mathrm{dB}}\eta}{d_s^2}(y_s - y_0), -\overline{d}_s\right]^T.\end{aligned} \tag{72}$$

Note that $\mathbf{g}'_s$ indicates that the last element of $\mathbf{g}_s$ was dropped. On the other hand, in the presence of noise, we cannot drop the dependence on p_0, since it does not cancel out in (21).

$$\begin{aligned}\mathbf{G}_{\mathrm{nc},q}^T &= [\mathbf{g}_1 - \mathbf{g}_S, \mathbf{g}_2 - \mathbf{g}_S, \ldots, \mathbf{g}_{S-1} - \mathbf{g}_S] \\ \mathbf{g}_s &\triangleq \gamma_s\left[\frac{e_{\mathrm{dB}}\eta}{d_s^2}(x_s - x_0), \frac{e_{\mathrm{dB}}\eta}{d_s^2}(y_s - y_0), -\overline{d}_s, 1\right]^T.\end{aligned} \tag{73}$$

Either $\mathbf{G}_q$ or $\mathbf{G}_{\mathrm{nc},q}$ is then inserted into (53), along with the correlation matrix of $\mathbf{q}$ from (25), yielding

$$\mathbf{J}_{\mathrm{drss}} = \sigma_{\mathrm{dB}}^{-2}\mathbf{G}_q^T\left(\mathbf{I}_{S-1} - S^{-1}\mathbf{1}_{S-1,1}\mathbf{1}_{S-1,1}^T\right)\mathbf{G}_q. \tag{74}$$

The CRLBs for RSS and DRSS are obtained by inverting (70) and (74), respectively. Though it is not obvious by inspection, the CRLB on $[x_0, y_0, \eta]$ for RSS (which is the top-left 3×3 submatrix of $\mathbf{J}^{-1}$) is identical to $\mathbf{J}_{\mathrm{drss}}^{-1}$ if and only if noise is ignored ($\tau \to -\infty$). Proving this is the subject of the remainder of this subsection.

Since all CRLBs in this paper are proportional to σ_{dB}^2, in this section we will omit it for notational simplicity. Ultimately, we are interested in the top-left 3×3 portion of $\mathbf{J}^{-1}$, since the noiseless bound for DRSS does not depend on p_0 and thus its CRLB will only be 3×3. In the noiseless case, $\gamma_s = 1$. Partitioning $\mathbf{G}$ and thus $\mathbf{J}$ for this case,

$$\mathbf{G} = \begin{bmatrix} \mathbf{A} & \mathbf{1} \\ \mathbf{c}^T & 1 \end{bmatrix} \tag{75}$$

$$\mathbf{J} = \begin{bmatrix} \mathbf{A}^T\mathbf{A} + \mathbf{c}\mathbf{c}^T & \mathbf{a} + \mathbf{c} \\ \mathbf{a}^T + \mathbf{c}^T & S \end{bmatrix} \tag{76}$$

where $\mathbf{A} \in \mathcal{R}^{(S-1)\times 3}$ and $\mathbf{c} \in \mathcal{R}^{3\times 1}$ contain appropriate elements of $\mathbf{G}$, and $\mathbf{a} = \mathbf{A}^T\mathbf{1}$. Using the Sherman-Morrison formula (a.k.a. the matrix inversion lemma) [26], the CRLB on $[x_0, y_0, \eta]$ for RSS is

$$[\mathbf{J}^{-1}]_{1:3,1:3} = [(\mathbf{A}^T\mathbf{A} + \mathbf{cc}^T) - (\mathbf{a}+\mathbf{c})S^{-1}(\mathbf{a}+\mathbf{c})^T]^{-1}. \tag{77}$$

The goal now is to show that the full 3 $\times$ 3 CRLB for DRSS is equivalent to (77).

Now note that the gradient matrix for DRSS is obtained from that of RSS via

$$\begin{aligned}\mathbf{G}_q &= \mathbf{G}(1:S-1, 1:3) - \mathbf{1}_{S-1,1}\mathbf{G}(S, 1:3) &(78)\\ &= \mathbf{A} - \mathbf{1c}^T. &(79)\end{aligned}$$

That expands the FIM in (74) to

$$\begin{aligned}\mathbf{J}_{\text{drss}} &\\ &= [\mathbf{A}^T - \mathbf{c1}^T]\left(\mathbf{I}_{S-1} - S^{-1}\mathbf{1}_{S-1,1}\mathbf{1}_{S-1,1}^T\right)[\mathbf{A} - \mathbf{1c}^T]\\ &= \mathbf{A}^T\mathbf{A} - \mathbf{ac}^T - \mathbf{ca}^T + (S-1)\mathbf{cc}^T\\ &\quad - S^{-1}(\mathbf{a} - (S-1)\mathbf{c})(\mathbf{a} - (S-1)\mathbf{c})^T\\ &= \mathbf{A}^T\mathbf{A} - \mathbf{ac}^T - \mathbf{ca}^T + (S-1)\mathbf{cc}^T\\ &\quad - S^{-1}(\mathbf{a} + \mathbf{c} - S\mathbf{c})(\mathbf{a} + \mathbf{c} - S\mathbf{c})^T\\ &= \mathbf{A}^T\mathbf{A} + \mathbf{cc}^T - S^{-1}(\mathbf{a}+\mathbf{c})(\mathbf{a}+\mathbf{c})^T \end{aligned} \tag{80}$$

Inverting (80) yields (77). Thus, the top-left 3 $\times$ 3 submatrix of the CRLB on $[x_0, y_0, \eta]$ based on RSS measurements is identical to the full 3 $\times$ 3 CRLB on $[x_0, y_0, \eta]$ based on DRSS measurements. In other words, no information is lost when compressing from S uncorrelated RSS measurements to $S-1$ correlated DRSS measurements. It is also of note that the derivations above are essentially unchanged if η is considered known.

Now reconsider the noisy case, wherein $\gamma_s < 1$. Now both FIMs are 4 $\times$ 4, since p_0 does not cancel out. We revise the partitioning to

$$\mathbf{G} = \begin{bmatrix}\mathbf{B}\\ \mathbf{d}^T\end{bmatrix}, \quad \mathbf{G}_q = \mathbf{B} - \mathbf{1d}^T. \tag{81}$$

where $\mathbf{B}$ and $\mathbf{d}$ are analogous to $\mathbf{A}$ and $\mathbf{c}$ from (75), but now include an additional column of $\mathbf{G}$. Since both FIMs are 4 $\times$ 4, we don't need to extract any 3 $\times$ 3 submatrices and can compare the two FIMs directly. The full FIM for RSS is

$$\mathbf{J}_{\text{rss}} = \mathbf{G}^T\mathbf{G} = \mathbf{B}^T\mathbf{B} + \mathbf{d}^T\mathbf{d}. \tag{82}$$

The FIM for DRSS parallels (80) with $\mathbf{A} \to \mathbf{B}$ and $\mathbf{c} \to \mathbf{d}$, hence

$$\begin{aligned}\mathbf{J}_{\text{drss}} &= (\mathbf{B}^T\mathbf{B} + \mathbf{dd}^T) + (-S^{-1}(\mathbf{b}+\mathbf{d})(\mathbf{b}+\mathbf{d})^T)\\ &= \underbrace{\mathbf{G}^T\mathbf{G}}_{\mathbf{J}_{\text{rss}}} \underbrace{- S^{-1}(\mathbf{G}^T\mathbf{11}^T\mathbf{G})}_{\mathbf{E}}\end{aligned} \tag{83}$$

where $\mathbf{b} = \mathbf{B}^T\mathbf{1}$ and $\mathbf{E}$ is an error term that vanishes as $S \to \infty$. Since we are subtracting a symmetric rank-one error term from $\mathbf{J}_{\text{rss}}$, again by the Sherman-Morrison formula,

$$\mathbf{J}_{\text{drss}}^{-1} = \mathbf{J}_{\text{rss}}^{-1} + \frac{\mathbf{G}^\dagger\mathbf{11}^T\mathbf{G}^{\dagger,T}}{S - \mathbf{1}^T\mathbf{GG}^\dagger\mathbf{1}}. \tag{84}$$

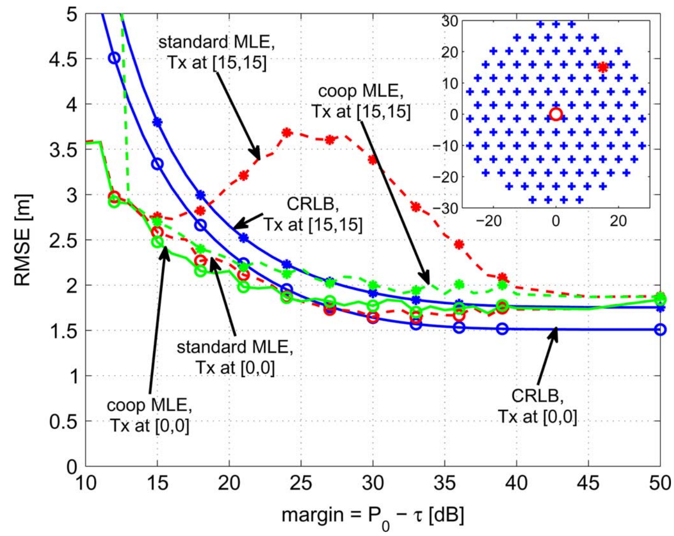

Fig. 9. RMSE of standard and cooperative MLE when the data was generated via the cooperative model. Both algorithms were given p_0 and η.

where $\mathbf{G}^\dagger$ is the left pseudo-inverse of $\mathbf{G}$. Equation (84) can be shown to have non-negative diagonal elements. Also, since $\text{tr}[\mathbf{AB}] = \text{tr}[\mathbf{BA}]$, it can be shown that the trace increases by

$$\text{tr}\left[\mathbf{J}_{\text{drss}}^{-1} - \mathbf{J}_{\text{rss}}^{-1}\right] = \frac{\mathbf{1}^T\mathbf{G}^{\dagger,T}\mathbf{G}^\dagger\mathbf{1}}{\mathbf{1}^T(\mathbf{I} - \mathbf{GG}^\dagger)\mathbf{1}}. \tag{85}$$

which is non-negative. Thus, the CRLB for DRSS is greater than that of RSS when background noise is accounted for, though perhaps not by much. This will be quantified in Section V.D.

V. Numerical RMSE and CRLB Evaluation

This section compares the new algorithms to existing methods, with a focus on determining the effects of the new models and unknown nuisance parameter values. In Sections V.A and V.B, we evaluate the performance of the MLE algorithms based on the new cooperative and non-cooperative RSS models, respectively. Their RMSE is compared to that of the MLE designed for a standard RSS model, when the actual simulated data is generated based on the new models. Section V.C shows the performance using measured non-cooperative data (all other subsections use simulated data). In Section V.D, we numerically evaluate the RMSE and CRLB for DRSS, when p_0 and η are unknown. Throughout this section, unless otherwise noted, $p_0 = 10$ dBm, $\eta = 2$, $\sigma_{\text{dB}} = 6$ dB, and $S = 129$ sensors (chosen since it leads to a convenient geometry as shown in Fig. 9). The noise levels τ_{coop} and τ_{nc} will be specified in each subsection, usually via the "margin" between p_0 and τ in the axes of each figure. The resolution for all grid searches is 0.5 m.

A. Cooperative RSS Simulations

Fig. 9 compares the performance of MLEs for the standard and cooperative model, with the data generated according to the cooperative model. The only difference between the MLEs is that the algorithm for the cooperative case exploits the lack of reports (represented as "NaNs") from sensors that could not demodulate the signal. Results are shown for two different trans-

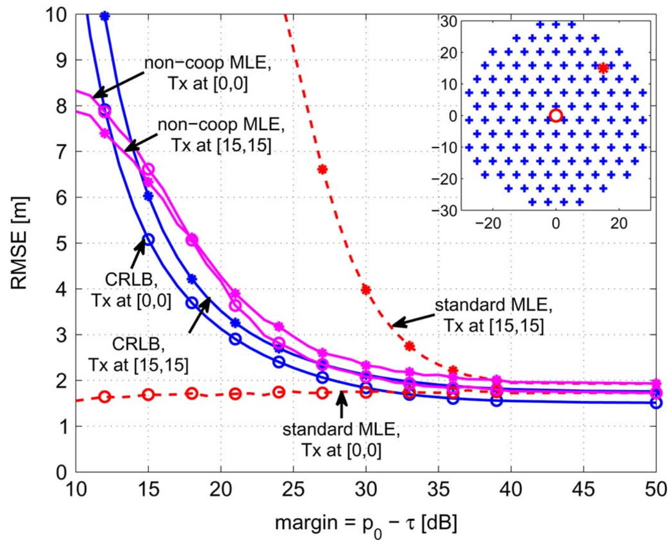

Fig. 10. RMSE of standard and non-cooperative MLE when the data was generated via the non-cooperative model. Both algorithms were given p_0 and η.

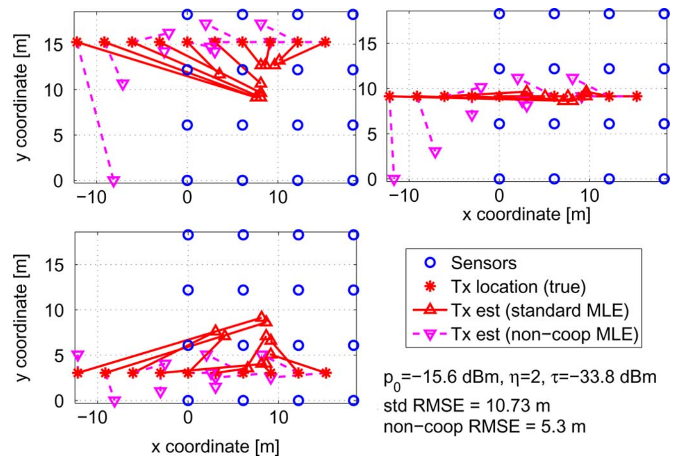

Fig. 11. Position estimates from measured non-cooperative RSS data. The lines connect each true transmitter position to the two position estimates from the standard MLE and the new non-cooperative MLE.

mitter placements, done one at a time. The horizontal axis indicates the margin between the transmitted power p_0 and the threshold $\tau_{\rm coop}$ below which the signal is not observed.

It is known that RSS measurements induce a bias in position estimates [30]. This may explain why the standard MLE sometimes does unexpectedly well, as when there is a poor model or inadequate data, the estimators appear to be biased, as indicated by the CRLB violations for low margins. This is also why the standard MLE appears to outperform the cooperative MLE at low margins, since at low margins the algorithm will guess near the origin by default, which happens to be the correct answer in one of our two scenarios. The authors have seen this effect many times in a variety of RSS localization scenarios, so bias should always be examined before interpreting results. On the other hand, for an asymmetric placement of the transmitter at $x_0 = y_0 = 15$ m, the exploitation of the NaN values by the cooperative MLE leads to a performance improvement. The standard MLE does well for margins of 15–20 dB because in that range, the only in-range sensors are roughly symmetric about the transmitter location, which relates to the bias issue noted above.

B. Non-Cooperative RSS Simulations

Fig. 10 compares the performance of MLEs for the standard and non-cooperative model, with the data generated according to the non-cooperative model. Again, results are shown for two different transmitter placements, done one at a time; and the horizontal axis indicates the margin between the transmitted power p_0 and the threshold $\tau_{\rm nc}$. Here, $\tau_{\rm nc}$ is the amount of noise power that is included in the RSS, in addition to whatever power is received from the transmitter.

Again, the effects of symmetry are evident in the results for $x_0 = y_0 = 0$. The symmetry appears to bias the standard MLE towards $(0, 0)$, so it performs unusually well when the transmitter happens to be near $(0, 0)$ and unusually poorly otherwise, indicating that the improper standard model decreases the estimator's robustness. On the other hand, the cooperative MLE performs consistently regardless of the transmitter placement, with a graceful degradation as the noise increases (margin decreases). The bias in the standard MLE is the reason it violates the CRLB.

Note that for both the cooperative and non-cooperative cases, performance distinctions are only evident for margins below 35 dB. However, as this paper focuses on locating weak emitters that may be far from many of the sensors, the case of low margins is exactly what we are interested in.

C. Non-Cooperative RSS Measurements

In this section, we present experimental localization performance for non-cooperative RSS measurements. The transmitter was a WARP FPGA board operating in the 2.4 GHz ISM band, and the receiver was a WiPry device connected to an IPod touch. As shown in Fig. 11, there were 16 sensors in a 4 $\times$ 4 grid, with 6.1 m between grid points. The transmitter was placed at 30 locations, and at each location, the position was estimated with both the standard MLE and the MLE based on the new non-cooperative model. Since the test area was a soccer field, we assumed $\eta = 2$, and the values of $p_0 = -15.6$ dBm and $\tau_{\rm nc} = -33.8$ dBm were measured directly. The resulting RMSE was 10.73 m for the standard MLE and 5.30 m for the proposed non-cooperative MLE.

D. Simulations With Unknown Values of p_0 and η

This section considers unknown p_0 and η. As such, DRSS methods should do well. A non-cooperative RSS model was assumed, though with a very low noise floor of $\tau_{\rm nc} = -50$ dBm.

Figs. 12 and 13 show the RMSE performance for several sets of algorithms: (i) standard MLE, MLE-DRSS, and LS-DRSS [11], all with known η; (ii) standard MLE and MLE-DRSS, with η estimated; (iii) LS-DRSS [11] with an incorrect value of η, off by $+0.5$; and (iv) LS-DRSS [11] with an incorrect value of η, off by -0.5. Performance of all methods in a group was effectively identical, since the noise floor was set so low here. In all cases, p_0 was unknown, and it was estimated by the standard MLE via (30). These results suggest that using a slightly incorrect value of η causes the LS-DRSS performance to be less reliable. Most of the time its performance degrades, though occasionally it improves.

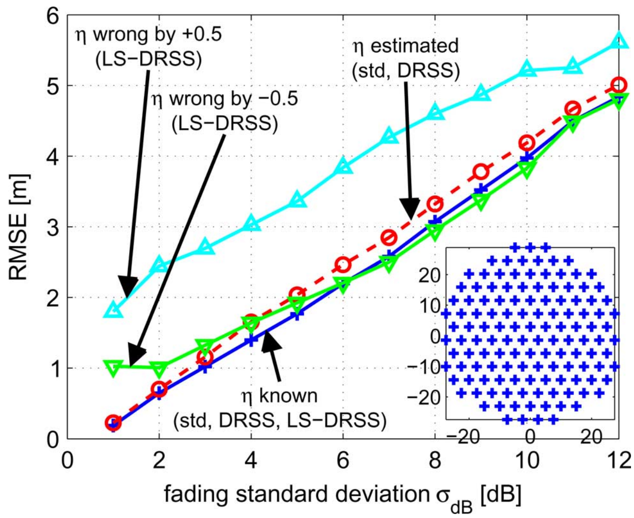

Fig. 12. Estimation performance when p_0 is unknown, for the uniform geometry (inset), averaged over 150 transmitter positions.

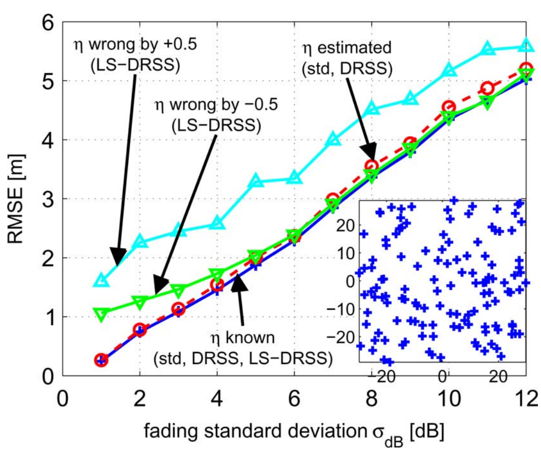

Fig. 13. Estimation performance when p_0 is unknown, for one realization of the random sensor positions (inset), averaged over 150 transmitter positions.

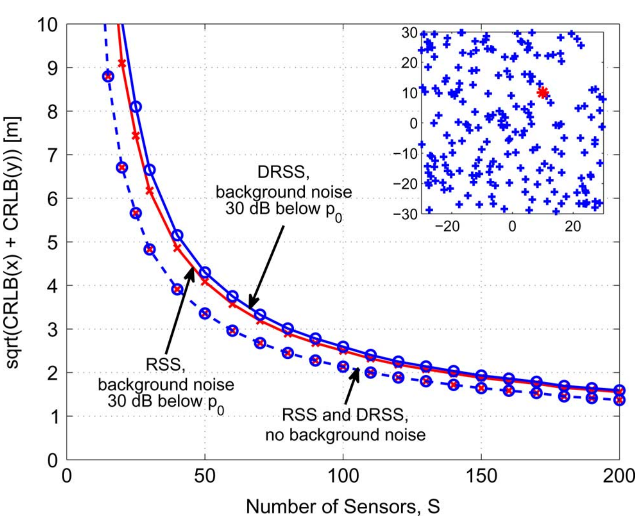

Fig. 14. CRLB of RSS and DRSS. The physical area was held constant and sensors were randomly placed within that area at increasing density. These results are averaged over 1000 trials, one of which is shown in the inset.

Fig. 14 shows a numerical comparison of the CRLB of RSS and DRSS, as derived in Section IV.B. The sensor geometry is a fixed coverage area but increasing density with random sensor placement. The noise level was $\tau_{\rm nc} = -20$ dBm. The upper and lower curves show the CRLB when the noise term γ_s is and is not included, respectively. The separation of the RSS and DRSS curves is very minor, and it disappears for large S. These results match the theoretical analysis in Section IV.B.

VI. Conclusion

This paper proposed new RSS models to account for the effects of weak signals and background noise, with particular attention on the non-cooperative case wherein little is known about the transmitted signal. These models were supported by extensive measured data. We also examined methods for mitigating nuisance parameters (transmit power and path loss), either by extending the MLEs to include them, or by using DRSS. The new models and algorithms were all rigorously analyzed to determine the effects of the models on the Fisher information content, and thus on the CRLB for positioning.

The impact of this work is that non-cooperative signals can be localized more accurately, based on the new models and associated algorithms. Partly this is due to reformulating the RSS model to account for noise, and partly this is because nuisance parameters are now dealt with rigorously. In practice, the transmitted power and path loss are not known in advance, and they are particularly difficult to obtain in non-cooperative source localization. The path loss parameter is now included in all of the MLEs whenever analytically tractable (as opposed to most existing work). The transmitted power was also included in the MLEs, but we also gave DRSS (which removes that parameter) a more rigorous treatment, and developed a much more computationally efficient estimation algorithm for DRSS.

Acknowledgment

The authors would like to thank Dr. M. Fickus of AFIT for his suggestions on the application of the Sherman–Morrison formula.

References

[1] A. J. Weiss, "On the accuracy of a cellular location system based on RSS measurements," *IEEE Trans. Veh. Technol.*, vol. 52, no. 6, pp. 1508–1518, Nov. 2003.

[2] R. A. Malaney, "Nuisance parameters and location accuracy in log-normal fading models," *IEEE Trans. Wireless Commun.*, vol. 6, no. 3, pp. 937–947, Mar. 2007.

[3] G. Mao, B. Fidan, and B. D. O. Anderson, "Wireless sensor network localization techniques," *Computer Netw.*, vol. 51, no. 10, pp. 2529–-2553, July 2007.

[4] A. H. Sayed, A. Tarighat, and N. Khajehnouri, "Network based wireless location," *IEEE Signal Process. Mag.*, vol. 22, no. 4, pp. 24–40, Jul. 2005.

[5] N. Patwari, J. N. Ash, S. Kyperountas, A. O. Hero, III, R. L. Moses, and N. S. Correal, "Locating the nodes: Cooperative localization in wireless sensor networks," *IEEE Signal Process. Mag.*, vol. 22, no. 4, pp. 54–69, Jul. 2005.

[6] R. K. Martin, R. Thomas, and Z. Wu, "Using spectral correlation for non-cooperative RSS-based positioning," in *Proc. Statist. Signal Process. Workshop*, Nice, France, Jun. 2011.

[7] N. Patwari, R. J. O'Dea, and Y. Wang, "Relative location in wireless networks," in *Proc. IEEE Veh. Technol. Conf.*, May 2001, vol. 2, pp. 1149–1153.

[8] D.-B. Lin, R.-T. Juang, and H.-P. Lin, "Robust mobile location estimation based on signal attenuation for cellular communication systems," in *Proc. IEEE Veh. Technol. Conf., 2005 Spring*, Stockholm, Sweden, May 2005, vol. 4, pp. 2425–2428.

[9] B.-C. Liu, K.-H. Lin, and J.-C. Wu, "Analysis of hyperbolic and circular positioning algorithms using stationary signal-strength-difference measurements in wireless communications," *IEEE Trans. Veh. Tech.*, vol. 55, no. 2, pp. 499–509, Mar. 2006.

[10] J. H. Lee and R. M. Buehrer, "Location estimation using differential RSS with spatially correlated shadowing," in *Proc. IEEE Global Telecommun. Conf.*, Honolulu, HI, Nov. 2009, pp. 1–6.

[11] S. Wang and R. Inkol, "Near-optimal least squares solution to received signal strength difference based geolocation," in *Proc. Int. Conf. Acoust., Speech, Signal Process.*, Prague, Czech Republic, May 2011.

[12] J. G. Proakis, *Digital Communications*, 3rd ed. Boston, MA: McGraw-Hill, Inc., 1995.

[13] G. Giorgetti, G. Gupta, and S. K. S. amd Manes, "Optimal RSS threshold selection in connectivity-based localization schemes," in *Proc. Int. Symp. Modeling, Analysis, Sim. Wireless Mobile Syst.*, Oct. 2008.

[14] L. Mailaender, "Geolocation bounds for received signal strength (RSS) in correlated shadow fading," in *Proc. IEEE Veh. Tech. Conf.*, Sep. 2011.

[15] T. S. Rappaport, *Wireless Communications: Principles and Practice*. Englewood Cliffs, NJ: Prentice-Hall, 1996.

[16] A. Dogandzic and P. P. Amran, "Signal-strength based localization in wireless fading channels," in *Proc. Asilomar Conf. Signals, Syst., Comput.*, Nov. 2004, pp. 2160–2164.

[17] N. Patwari and P. Agrawal, "Effects of correlated shadowing: Connectivity, localization, and RF tomography," in *Proc. IEEE/ACM Int. Conf. Info. Process. Sensor Netw. (IPSN)*, St. Louis, MO, Apr. 2008, pp. 82–93.

[18] Y. Sheng, K. Tan, G. Chen, D. Kotz, and A. Campbell, "Detecting 802.11 MAC layer spoofing using received signal strength," in *Proc. 27th Annu. Joint Conf. IEEE Comput. Commun. Soc. (INFOCOM)*, Apr. 2008, pp. 1768–1776.

[19] J.-C. Chen, "Improved maximum likelihood location estimation accuracy in wireless sensor networks using the cross-entropy method," in *Proc. Int. Conf. Acoust., Speech, Signal Process.*, Taipei, Taiwan, Apr. 2009, pp. 1325–1328.

[20] K. Bauer, D. McCoy, E. W. Anderson, D. Grunwald, and D. C. Sicker, "CRAWDAD trace cu/rssi/text/omni_16dbm (v. 2009-05-28)," Jul. 2010 [Online]. Available: http://crawdad.cs.dartmouth.edu/cu/rssi/text/omni_16dbm

[21] X. Sheng and Y.-H. Hu, "Maximum likelihood multiple-source localization using acoustic energy measurements with wireless sensor networks," *IEEE Trans. Signal Process.*, vol. 53, no. 1, pp. 44–53, Jan. 2005.

[22] C. Y. Kim, D. Song, Y. Xu, and J. Yi, "Localization of multiple unknown transient radio sources using multiple paired mobile robots with limited sensing ranges," in *Proc. IEEE Int. Conf. Robot. Autom. (ICRA)*, Shanghai, China, May 2011.

[23] WARP FPGA Board, Rice University [Online]. Available: http://warp.rice.edu/trac/wiki/FPGA%20Board

[24] MetaGeek, "Wi-Spy 2.4i spectrum analyzer," [Online]. Available: http://www.metageek.net/products/wi-spy-24i

[25] G. H. Golub and C. F. Van Loan, *Matrix Computations*. Baltimore, MD: The Johns Hopkins Univ. Press, 1996.

[26] S. M. Kay, *Fundamentals of Statistical Signal Processing: Estimation Theory*. Englewood Cliffs, NJ: Prentice Hall, 1993.

[27] F. Gustafsson, F. Gunnarsson, and D. Lindgren, "Sensor models and localization algorithms for sensor networks based on received signal strength," *EURASIP J. Wireless Commun. Netw.*, vol. 2012, Jan. 2012.

[28] F. Gini, R. Reggiannini, and U. Mengali, "The modified CramerRao bound in vector parameter estimation," *IEEE Trans. Commun.*, vol. 46, pp. 52–60, Jan. 1998.

[29] R. Munroe, xkcd, Riemann-Zeta, Sep. 30, 2011 [Online]. Available: http://www.xkcd.com/113

[30] N. Patwari, A. O. Hero, III, M. Perkins, N. S. Correal, and R. J. O'Dea, "Relative location estimation in wireless sensor networks," *IEEE Trans. Signal Process.*, vol. 51, no. 8, pp. 2137–2148, Aug. 2003.

[31] R. K. Martin, A. King, R. Thomas, and J. Pennington, "Practical limits in RSS based positioning," in *Proc. Int. Conf. Acoust., Speech, Signal Process.*, Prague, Czech Republic, May 2011.

Richard K. Martin received dual B.Sc. degrees (*summa cum laude*) in physics and electrical engineering from the University of Maryland, College Park, in 1999, and the M.S. and Ph.D. degrees in electrical engineering from Cornell University, Ithaca, NY, in 2001 and 2004, respectively.

Since August 2004, he has been with the Department of Electrical and Computer Engineering, Air Force Institute of Technology (AFIT), Dayton, OH, where he is an Associate Professor. He is the author of 26 journal papers and 53 conference papers, and he holds five patents. His research interests include navigation and source localization, radio tomographic imaging, cognitive radio, and laser radar.

Dr. Martin has been elected Electrical and Computer Engineering Instructor of the Quarter three times and HKN Instructor of the Year twice by the AFIT students.

Amanda Sue King received the B.Sc. degree in statistics from Eastern Kentucky University, Richmond, in 2005, and the M.Sc. degree in applied statistics from Wright State University, Dayton, OH, in 2009. She is currently working towards the Ph.D. degree in electrical engineering at the Air Force Institute of Technology (AFIT), Dayton, OH, where her research focus is source localization using received signal strength and statistical signal processing.

Jason R. Pennington received the B.Sc. degree in computer engineering and the M.Sc. degree in computational science from Miami University, Miami, in 2009 and 2011, respectively. Since May 2011, he has been working toward the Ph.D. degree in electrical engineering at the Air Force Institute of Technology (AFIT), Dayton, OH.

His research interests include cognitive radio and MIMO communications.

Ryan W. Thomas received the B.Sc. degree from Harvey Mudd College, Claremont, CA, in 1999, the M.Sc. degree in computer engineering from the Air Force Institute of Technology, Wright-Patterson, OH, in 2001, and the Ph.D. degree in computer engineering from Virginia Polytechnic Institute and State University, Blacksburg, in 2007.

He is currently an Adjunct Professor of Computer Engineering in the Department of Electrical and Computer Engineering at the Air Force Institute of Technology. He previously worked at the Air Force Research Laboratory, Sensors Directorate as a Digital Antenna Array Engineer.His research focuses on the design, architecture and evaluation of cognitive networks, cognitive radios, and software defined radios.

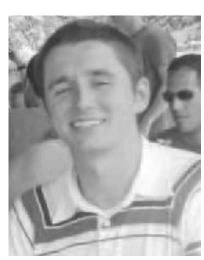

Russell Lenahan received the B.Sc. degree from the University of Dayton, Dayton, OH, in 2011. He was working toward the M.Sc. degree at the Air Force Institute of Technology when this work was performed.

He died shortly after this work was completed. His contribution to this work, particularly in programming the sensors, was invaluable, and he will be missed.

Cody Lawyer is currently working toward the M.Sc. degree in electrical engineering at Wright State University, Dayton, OH.

His research interests include signal processing and communications.